Estimating Effective Collision Frequency and Kinetic Entropy Uncertainty in Particle-in-Cell Simulations

Journal of Physics: Conference Series **1620** (2020) 012009 doi:10.1088/1742-6596/1620/1/012009

Estimating Effective Collision Frequency and Kinetic Entropy Uncertainty in Particle-in-Cell Simulations

Haoming Liang[1,2], **P. A. Cassak**[2], **M. Swisdak**[3], **Sergio Servidio**[4]

[1] Center for Space Plasma and Aeronomic Research, University of Alabama in Huntsville, Huntsville, AL 35899, USA
[2] Department of Physics and Astronomy, West Virginia University, Morgantown, WV 26506, USA
[3] Department of Physics and Institute for Research in Electronics and Applied Physics, University of Maryland, College Park, MD 20740, USA
[4] Dipartimento di Fisica, Università della Calabria, I-87036 Cosenza, Italy

E-mail: haoming.liang@uah.edu

Abstract. A kinetic entropy diagnostic was systematically developed for fully kinetic collisionless particle-in-cell (PIC) simulations in Liang et al., Phys. Plasmas **26**, 082903 (2019). Here, we first show that kinetic entropy can be used to quantitatively evaluate numerical dissipation in the PIC simulation. Assuming numerical effects can be treated using a relaxation time approximation collision operator, the rate of increase of the kinetic entropy is related to the kinetic entropy. The effective collision frequency due to numerical effects is then easy to evaluate in a collisionless PIC simulation. We find an effective collision frequency of approximately a tenth of the ion cyclotron frequency. This could have important implications for collisionless PIC simulation studies of magnetic reconnection, plasma turbulence, and collisionless shocks. Then, we analyze the uncertainty of the local kinetic entropy density at different locations as a function of the chosen velocity space grid. We find that although the numerically obtained kinetic entropy density varies significantly for small or large velocity space grids, there is a range for which the kinetic entropy density is only weakly sensitive to the velocity space grid. Our analysis of the uncertainty suggests a velocity space grid close to the thermal velocity is optimal, and the uncertainty introduced is significantly less than the physical change in kinetic entropy density.

1. Introduction

Understanding how energy is dissipated via fundamental plasma processes is crucial in many astrophysical, heliospheric, and planetary studies. In settings for which the plasma is nearly collisionless, dissipation often occurs via plasma processes such as magnetic reconnection [1, 2, 3], plasma turbulence [4, 5], and collisionless shocks [6]. Although the ability to investigate these plasma processes observationally, experimentally, numerically, and theoretically is improving, identifying when and where dissipation occurs is still a key challenge [3, 7].

Entropy is a natural candidate to identify and quantify dissipation because for closed systems it is conserved in the absence of dissipation and is non-decreasing in time when dissipation is present. In the kinetic description, kinetic entropy is a measure of the number of ways to arrange particles in the plasma to produce a given distribution of plasma in phase space [8, 9]. If distribution functions are isotropic, the fluid/thermodynamic form of entropy per

particle is related to p/ρ^{γ}, where p is the scalar pressure, ρ is the mass density, and γ is the ratio of specific heats. The fluid form has been used to study numerous plasma systems [10, 11, 12, 13, 14, 15, 16, 17, 18, 19, 20].

Due to the fact that many astrophysical, heliophysical, and planetary plasmas are weakly collisional, distribution functions can strongly deviate from isotropy, especially when the system dynamics has spatial or temporal structure at kinetic scales (at and below the gyroradius of charged particles in magnetic fields). Within the gyrokinetic model, the perturbed kinetic entropy is related to the square of the perturbed distribution function [21, 22, 23], which has been used to analyze magnetic reconnection [24, 25] and plasma turbulence [26, 27, 28, 29, 30, 31, 32, 33, 34]. There are settings for which the physical system does not obey the gyrokinetic description, such as when distribution functions are significantly non-gyrotropic [35, 36, 37]. Thus, studying kinetic entropy without any degrees of freedom integrated out is important. Kinetic entropy in full generality has been investigated in observational [38, 39, 40, 41, 42] and theoretical [43, 44] studies. The kinetic entropy has also been employed in particle-in-cell (PIC) simulations to study plasma turbulence [45] and magnetic reconnection [46], the latter of which we refer to as Study 1.

Despite these efforts, there are challenges to understand entropy production in real systems using theory and simulations. For example, associating entropy production with dissipation requires a closed system, but natural systems tend not to be closed. Also, a local increase of kinetic entropy density could be due to convection of inhomogeneous plasma parameters such as density or temperature rather than being due to dissipation, making the recognition of dissipation ambiguous. In numerical studies, numerical errors in simulations effectively generate a spurious change in entropy, making the simulation results potentially unphysical and complicating comparisons between simulations and observations. In this study, we address two numerical aspects of kinetic entropy in PIC simulations.

Study 1 performed a systematic analysis of the kinetic entropy diagnostic in fully kinetic PIC simulation from first principles. The kinetic entropy was calculated for a simple case of collisionless two-dimensional (2D) anti-parallel magnetic reconnection with periodic boundary conditions in order to examine how accurately a collisionless PIC simulation conserves kinetic entropy in a closed system. They found that for a simulation with total energy showing excellent conservation – it only increased by 0.24% – the relative changes of the kinetic entropy were about 4.5%, 2.1% and 3.2% for electrons, ions, and total, respectively. This level conservation is reasonably good; by comparison nearly one-third of the electromagnetic energy was converted into particle kinetic energy over the same time.

Interestingly, Study 1 reported that kinetic entropy monotonically increased in time, which is what one would expect for an explicit physical collision operator. As there were no physical collisions in the simulation, the increase of kinetic entropy is purely due to numerical effects. As the kinetic entropy was non-decreasing, the effective numerical kinetic entropy production in some way mimicked physical collisions. This suggests that it would be useful to quantify the effective collisionality due to numerical aspects of the simulation. Doing so would allow simulation users to better understand the effective collisions in their simulations, and to provide a baseline necessary to overcome in order to study physical collisions for codes including an explicit collision operator.

An analogous approach has long been used in magnetohydrodynamics (MHD) simulations, especially in global simulations of the solar corona (*e.g.*, [47, 48]) and planetary magnetospheres (*e.g.,* [48, 49, 50, 51, 52]), where the numerical algorithm introduces an effective dissipation to ensure convergence (*e.g.,* [53]). One approach to quantifying the numerical effective resistivity in such MHD simulations is to investigate the properties of magnetic reconnection that happens due to numerical dissipation at the grid (*e.g.,* [48, 54]). In this study, we argue that kinetic entropy measured in a PIC simulation can be a useful tool to estimate the effective collision

frequency due to numerical effects. We find the effective collision frequency to be approximately a tenth of the ion cyclotron frequency for the simulation in Study 1. Other approaches have been used to estimate effective collision frequencies, especially in the early days of PIC simulations, (*e.g.,* [55, 56, 57, 58, 59, 60]).

Study 1 also included an effort to validate the kinetic entropy diagnostic and explore relevant numerical parameters for proper usage of the diagnostic. They examined the velocity space grid and the number of macro-particles per grid cell. For the velocity space grid Δv, the uncertainty of the measured kinetic entropy is quite sensitive to the selection of the velocity grid size. Study 1 reported that a velocity space grid of approximately the species thermal speed gives a kinetic entropy integrated over the entire domain that is close to the predicted value at the initial time when all the distribution functions were Maxwellian. However, they did not present how the grid affects the accuracy of local measurements of the kinetic entropy from non-Maxwellian distributions. This is important because even if the velocity space grid is chosen to give accurate results at the initial time, there is no assurance it is still sufficient at later times. Here, we present an analysis of the uncertainty due to the choice of the velocity space grid on the calculation of the local kinetic entropy density for non-Maxwellian distributions at late time in the simulation of Study 1.

We organize this paper as follows: Sec. 2 discusses a relation between kinetic entropy and a modeled effective collision frequency in the simulations. Sec. 3 uses the PIC simulation results from Study 1 to quantify the effective collision frequency and assess the reliability of the kinetic entropy measurements as a function of velocity space grid. Sec. 4 summarizes the conclusions and implications of this study.

2. Kinetic Entropy and Effective Collision Frequency

In this section, we derive a relation between the kinetic entropy and the effective collision frequency. The continuous Boltzmann entropy density $s(\vec{r},t)$ is defined as

$$s(\vec{r},t) = -k_B \int d^3v f(\vec{r},\vec{v},t) \left[\ln f(\vec{r},\vec{v},t)\right]. \tag{1}$$

From the Boltzmann equation, $df(\vec{r},\vec{v},t)/dt = C[f(\vec{r},\vec{v},t)]$, where $C[f(\vec{r},\vec{v},t)]$ is a collision operator containing both inter- and intra-species collisions, one can derive an evolution equation for $s(\vec{r},t)$ (*e.g.,* [44]):

$$\frac{\partial s(\vec{r},t)}{\partial t} + \nabla \cdot \vec{\mathcal{J}}(\vec{r},t) = -k_B \int d^3v C[f(\vec{r},\vec{v},t)][1 + \ln f(\vec{r},\vec{v},t)], \tag{2}$$

where $\vec{\mathcal{J}}(\vec{r},t) = -k_B \int d^3v \vec{v} f(\vec{r},\vec{v},t) \ln f(\vec{r},\vec{v},t)$ is the entropy flux. This is a continuity equation of kinetic entropy and the right hand side, related to the collision operator, is a source term.

To represent the numerical production of kinetic entropy, we assume a Bhatnagar-Gross-Krook type relaxation time collision operator [61]. The original version was of the form $C[f(\vec{r},\vec{v},t)] = -\nu[f(\vec{r},\vec{v},t) - f_0(\vec{r},\vec{v},t)]$, where $f_0(\vec{r},\vec{v},t)$ is an equilibrium distribution function and ν is a constant collision frequency whose inverse sets the time scale of the relaxation of $f(\vec{r},\vec{v},t)$ to $f_0(\vec{r},\vec{v},t)$. This operator lacks conservation law properties required of collision operators, but gives a simplified operator that does reasonably well for distributions that do not differ greatly from Maxwellian distributions. We employ a modified relaxation time collision operator of

$$C[f(\vec{r},\vec{v},t)] = -\nu(\vec{r},t)[f(\vec{r},\vec{v},t) - f_M(\vec{r},\vec{v},t)], \tag{3}$$

for which the collision frequency $\nu(\vec{r},t)$ can be a function of space and time, and the equilibrium distribution $f_0(\vec{r},\vec{v},t)$ is replaced by the local Maxwellianized $f_M(\vec{r},\vec{v},t)$ defined as a Maxwellian distribution with density $n(\vec{r},t)$, bulk flow velocity $\vec{u}(\vec{r},t)$, and temperature $T(\vec{r},t)$ equivalent

to those of the local distribution function $f(\vec{r},\vec{v},t)$. Physically, this collision operator drives distribution functions towards a Maxwellian with the local bulk properties, but if the system dynamics changes the bulk properties at a given position it will then relax to the new Maxwellianized distribution rather than an unknown equilibrium distribution $f_0(\vec{r},\vec{v},t)$. We stress that this operator is used for expediency, not based on any evidence that the numerical dissipation in a PIC simulation follows this collision operator.

Inserting the collision operator in Eq. (3) into Eq. (2), defining $\delta f(\vec{r},\vec{v},t) = f(\vec{r},\vec{v},t) - f_M(\vec{r},\vec{v},t)$, and noting that $\int d^3v \delta f(\vec{r},\vec{v},t) = 0$ because the density associated with $f_M(\vec{r},\vec{v},t)$ is the same as the total density from $f(\vec{r},\vec{v},t)$ by definition, straight-forward manipulations give

$$\frac{\partial s(\vec{r},t)}{\partial t} + \nabla\cdot\vec{\mathcal{J}}(\vec{r},t) = \nu(\vec{r},t)k_B\int d^3v\delta f(\vec{r},\vec{v},t)\left[\ln f_M(\vec{r},\vec{v},t) + \ln\left(1+\frac{\delta f(\vec{r},\vec{v},t)}{f_M(\vec{r},\vec{v},t)}\right)\right]. \quad (4)$$

The integral in the first term on the right, proportional to $\int d^3v\delta f(\vec{r},\vec{v},t)\ln f_M(\vec{r},\vec{v},t)$, is also zero because $\ln f_M(\vec{r},\vec{v},t)$ brings down a factor proportional to $[\vec{v}-\vec{u}(\vec{r},t)]^2$, so the result is the difference between the actual and Maxwellianized temperatures, which again is zero by definition. Since the relaxation time collision operator is only valid if $\delta f(\vec{r},\vec{v},t)$ is small, we do an expansion in powers of $\delta f(\vec{r},\vec{v},t)$. The leading term is second order,

$$\frac{\partial s(\vec{r},t)}{\partial t} + \nabla\cdot\vec{\mathcal{J}}(\vec{r},t) = \nu(\vec{r},t)k_B\int d^3v\left(\frac{[\delta f(\vec{r},\vec{v},t)]^2}{f_M(\vec{r},\vec{v},t)} + \mathcal{O}(\delta f^3)\right), \quad (5)$$

where $\mathcal{O}(\delta f^3)$ indicates equal or higher order terms than δf^3. On the other hand, defining $s_M(\vec{r},t)$ as the kinetic entropy from Eq. (1) evaluated with the Maxwellian distribution function $f_M(\vec{r},\vec{v},t)$, we see that

$$\begin{aligned} s_M(\vec{r},t) - s(\vec{r},t) &= -k_B\int d^3v f_M(\vec{r},\vec{v},t)\ln f_M(\vec{r},\vec{v},t) + k_B\int d^3v f(\vec{r},\vec{v},t)\ln f(\vec{r},\vec{v},t) \\ &= k_B\int d^3v[f_M(\vec{r},\vec{v},t)+\delta f(\vec{r},\vec{v},t)]\ln\left(1+\frac{\delta f(\vec{r},\vec{v},t)}{f_M(\vec{r},\vec{v},t)}\right) \\ &= k_B\int d^3v\left(\frac{[\delta f(\vec{r},\vec{v},t)]^2}{2f_M(\vec{r},\vec{v},t)} + \mathcal{O}(\delta f^3)\right). \end{aligned} \quad (6)$$

This quantity, quadratic in $\delta f(\vec{r},\vec{v},t)$, resembles the ϵ and enstrophy parameters introduced in Refs. [62] and [63], respectively. Comparing Eqs. (5) and (6), we find

$$\frac{\partial s(\vec{r},t)}{\partial t} + \nabla\cdot\vec{\mathcal{J}}(\vec{r},t) = 2\nu(\vec{r},t)\left[s_M(\vec{r},t) - s(\vec{r},t)\right] + \mathcal{O}(\delta f^3). \quad (7)$$

Integrating this equation over all position space gives

$$\frac{dS(t)}{dt} \simeq 2\int d^3r\nu(\vec{r},t)\left[s_M(\vec{r},t) - s(\vec{r},t)\right], \quad (8)$$

where $S(t) = \int d^3r s(\vec{r},t)$ is the total entropy. Finally, we define the effective collision frequency $\nu_{\rm eff}$ as the average collision frequency weighted by the departure from Maxwellianity,

$$\nu_{\rm eff}(t) = \frac{\int d^3r\nu(\vec{r},t)\left[s_M(\vec{r},t) - s(\vec{r},t)\right]}{\int d^3r\left[s_M(\vec{r},t) - s(\vec{r},t)\right]}. \quad (9)$$

Then,

$$\frac{dS(t)}{dt} \simeq 2\nu_{\rm eff}(t)\int d^3r\left[s_M(\vec{r},t) - s(\vec{r},t)\right], \quad (10)$$

Thus, within the confines of the assumptions that $\delta f(\vec{r},\vec{v},t)$ is small and the relaxation time approximation is reasonable, we find the difference between the local kinetic entropy density and its value for its equivalent equilibrium distribution function is a source of kinetic entropy. Since the Maxwellian distribution is the maximum entropy state for a given number of particles and energy, $s_M(\vec{r},t) \geq s(\vec{r},t)$, and any non-Maxwellian distribution is associated with a positive collision frequency, as expected. The utility of writing the kinetic entropy evolution in this way is that it is straightforward to calculate $dS(t)/dt$ and $\int d^3r\,[s_M(\vec{r},t) - s(\vec{r},t)]$ in PIC simulations, which allows us to calculate the effective relaxation collision frequency $\nu_{\rm eff}(t)$.

3. Results

The results in this section are generated from the same simulation in Study 1. Details of the simulation setup are available in Study 1.

3.1. Effective Collision Frequency of Collisionless PIC Simulation

Here, we use the formalism discussed in Sec. 2 to estimate the effective collision frequency $\nu_{\rm eff}(t)$ in the simulation. From Eq. (10), we need the time rate of change of the kinetic entropy $dS(t)/dt$ and the spatial integral of $s_M(\vec{r},t) - s(\vec{r},t)$. In principle, this can be carried out for each species individually or for the plasma as a whole.

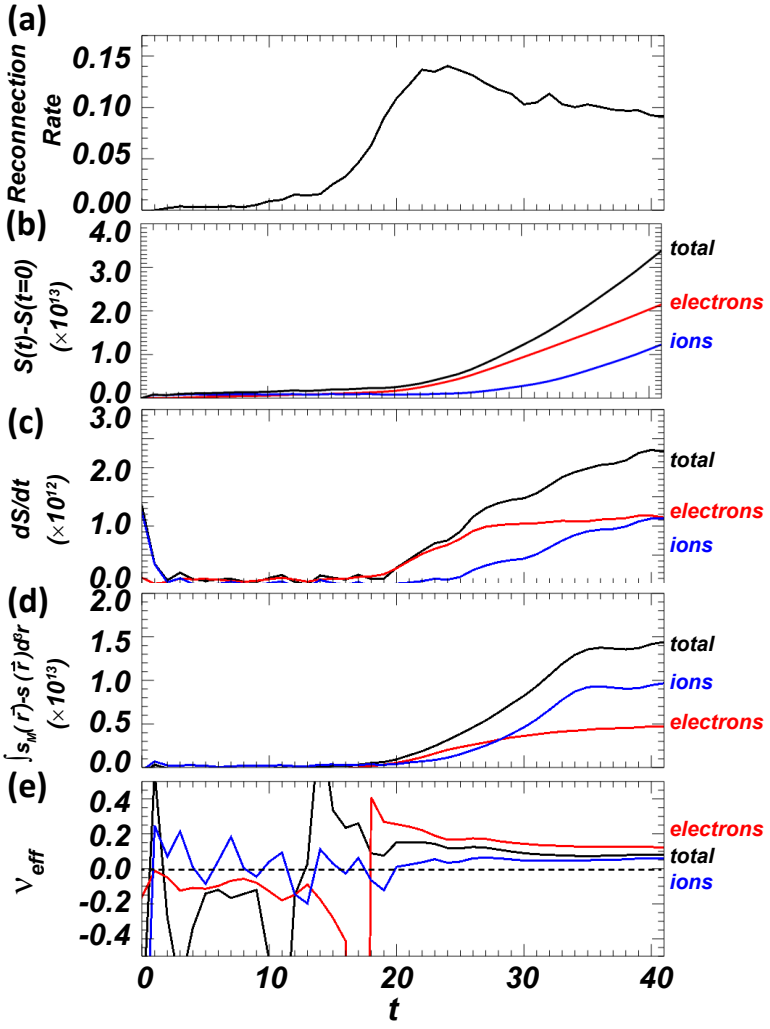

Figure 1. Determination of effective collision frequency in the PIC simulation. The plots show the time t evolution of the (a) reconnection rate, (b) kinetic entropy $S(t)$ relative to its initial value $S(0)$, (c) time rate of change of the kinetic entropy $dS(t)/dt$, (d) spatially integrated $s_M(\vec{r},t) - s(\vec{r},t)$, and (e) the associated effective collision frequency $\nu_{\rm eff}(t)$ calculated from Eq. (10). In (b)-(e), the colors are for electrons (red), ions (blue), and their sum (black). Panel (a) is reproduced from Liang et al., Phys. Plasmas **26**, 082903 (2019), with the permission of AIP Publishing.

To put the time evolution of the system in perspective, Fig. 1(a) shows the reconnection rate in units of $v_{A,up}B_0$, where B_0 is the asymptotic magnetic field and $v_{A,up}$ is the Alfvén speed at the upstream edge of the diffusion region, as a function of time t in units of the inverse ion cyclotron frequency Ω_{ci}^{-1} based on B_0, which was previously shown in Study 1. Reconnection begins in earnest just before $t = 20\ \Omega_{ci}^{-1}$. Panel (b) shows the kinetic entropy $S(t)$ relative to its initial value $S(0)$ in units of k_B as a function of time t, and panel (c) shows its time rate of change. In both plots, the kinetic entropy of electrons is in red, ions in blue, and the total (their sum) in black. The brief period at the beginning of the simulation where the ion kinetic entropy increases relatively rapidly is because the initial current sheet thickness is 0.5 ion inertial scales, so the ions in the current sheet self-adjust to a wider sheet until about $t = 2\ \Omega_{ci}^{-1}$. Electrons do not show such an effect because their gyro-radius is smaller than the current sheet thickness, so their adjustment is smaller. From $t = 2 - 20\ \Omega_{ci}^{-1}$, the system is relatively quiet and numerical kinetic entropy production is small. The rate of change of kinetic entropy begins to increase when the reconnection begins in earnest around $t = 20\ \Omega_{ci}^{-1}$, and continues increasing for nearly the duration of the simulation.

The time rate of change of kinetic entropy shows different behavior for electrons and ions during reconnection. The electron kinetic entropy increases before the ion kinetic entropy, reaching a nearly steady rate for $t > 27\ \Omega_{ci}^{-1}$, while the ion kinetic entropy increases more slowly, reaching a nearly steady rate later in time at $t = 37\ \Omega_{ci}^{-1}$. Physically, the electrons develop non-Maxwellian distributions more rapidly than ions during the reconnection process, which makes sense as it takes time for the micro-scale processes allowing reconnection to fully couple to the larger (ion) scales.

The value of $\int d^3r[s_M(\vec{r},t) - s(\vec{r},t)]$ is shown in units of k_B as a function of time t in panel (d). The values for ions, electrons, and total are close to zero for $t < 20\ \Omega_{ci}^{-1}$ since the distributions are initially Maxwellian. When reconnection begins in earnest at $t = 20\ \Omega_{ci}^{-1}$, the integrals start to increase, which means the velocity distributions start to become non-Maxwellian during reconnection. The difference between electrons and ions shows that electrons become non-Maxwellian earlier than ions when reconnection begins, which is consistent with the discussion of panel (b) and is reasonable because electrons are more easily influenced by the reconnection process due to their small mass. The ion distributions become more non-Maxwellian at later times, probably due to the much larger non-adiabatic-motion regions than electrons. Note that the different initial temperatures for electrons and ions could lead to different magnitudes of $\int d^3r[s_M(\vec{r},t) - s(\vec{r},t)]$.

Panel (e) shows the resultant effective collision frequency $\nu_{\text{eff}}(t)$ calculated from Eq. (10) as a function of time t for electrons (red), ions (blue), and total (black) in units of Ω_{ci}. Up until $t = 20\ \Omega_{ci}^{-1}$, ν_{eff} is the ratio of two small numbers so there are large spurious spikes around the expected value near zero; this time period should be ignored. After reconnection starts in earnest around $t = 20\ \Omega_{ci}^{-1}$, the results are relatively smooth. The approximate values of ν_{eff} in the relatively steady phase ($t = 33 - 41\ \Omega_{ci}^{-1}$) are 0.12 Ω_{ci} for electrons, 0.05 Ω_{ci} for ions, and 0.07 Ω_{ci} for the total.

3.2. Uncertainty of Kinetic Entropy Diagnostic

Assessing the uncertainty of kinetic entropy as measured numerically in a PIC simulation requires comparing simulation results with different velocity space grids Δv. One aspect of this was carried out in Study 1, where the total kinetic entropy S was compared for different Δv. Since the kinetic entropy is not explicitly evolved in the PIC evolution equations, the simulations with different velocity space grids behave identically in terms of particle trajectories, velocities, and electromagnetic fields; the only difference is the way in which the kinetic entropy is evaluated. The results from that study are reproduced in Fig. 2.

Panel (a) shows the total initial electron (black) and ion (blue) kinetic entropy $S(t = 0)$

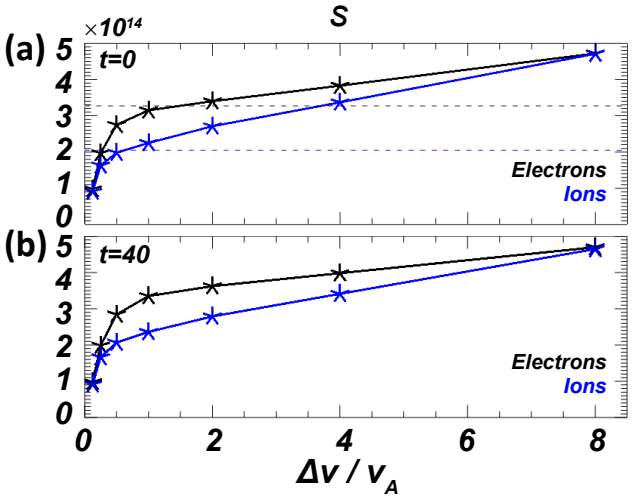

Figure 2. Kinetic entropy S for electrons (black) and ions (blue) in seven simulations with $\Delta v/v_A = 0.125, 0.25, 0.5, 1.0, 2.0, 4.0, 8.0$ (a) at $t = 0$ and (b) at $t = 40\ \Omega_{ci}^{-1}$. The dashed lines in (a) indicate the analytical values at $t = 0$ for electrons (black) and ions (blue). Reproduced from Liang et al., Phys. Plasmas **26**, 082903 (2019), with the permission of AIP Publishing.

in units of k_B as a function of Δv in units of v_A, where v_A is the Alfvén speed based on B_0 and the initial current sheet density. The simulation from Study 1 is initialized with drifting Maxwellian distributions everywhere in space, so the numerically calculated kinetic entropy at $t = 0$ was verified by comparing it with analytical expressions of kinetic entropy for Maxwellian distributions. These values are shown as the horizontal dashed lines in panel (a). This method was used to identify an optimal Δv for the kinetic entropy calculation, at least at $t = 0$. It was found that for both electrons and ions, the velocity space grid giving the best agreement with the analytical calculation is near the species thermal speed.

As mentioned in the introduction and in Study 1, validating the entropy calculation at $t = 0$ does not ensure the selected velocity space grid size is appropriate at later times. Panel (b) shows an analogous plot as panel (a), but at $t = 40\ \Omega_{ci}^{-1}$ near the end of the simulation. The overall trend in S with varying Δv is similar to that at $t = 0$, but there is no direct way to assess if the velocity space resolution remains sufficient.

Here, we examine the effect of the velocity space grid, but using a locally measured distribution function instead of the total kinetic entropy found from integrating over the whole domain. To do so, we assess the velocity space grid dependence on the most non-Maxwellian distribution at late times ($t = 41\ \Omega_{ci}^{-1}$ in the simulation); this presumably provides the upper limit of the uncertainty for the kinetic entropy calculation.

For the simulation in Study 1, the most non-Maxwellian distribution, *i.e.,* the $\vec{r}$ location where $s_M(\vec{r}, t) - s(\vec{r}, t)$ is a maximum, occurs at the X-point at late time. Physically, it is associated with electron meandering orbits, such as those displayed in Fig. 4 of Ref. [64]. Its projection is shown in the $v_x - v_y$ plane in Fig. 3(h). This distribution function has sharp structure in the v_z direction (not shown) and therefore should be the hardest to resolve in velocity space, so the uncertainty of its kinetic entropy density should be the greatest.

We calculate the electron kinetic entropy density s_e for this local distribution function as a function of velocity space grid Δv. The results are shown in Fig. 3(a), which represents the local counterpart to the global result in Fig. 2. The black curve is for $t = 0$ for a Maxwellian distribution in the upstream region, while the blue curve is for the distribution at the X-point at $t = 41\ \Omega_{ci}^{-1}$. As for the global measure, there is a medium range denoted by the blue and black rectangles between about 0.5 v_A and 2 v_A where the kinetic entropy of the Maxwellian plasma is not strongly dependent on the velocity space grid. The analytical value of the kinetic entropy for this case is shown as the horizontal red dashed line. The uncertainty in the kinetic entropy density as a result of the velocity space grid within this range is approximately 15%, in spite

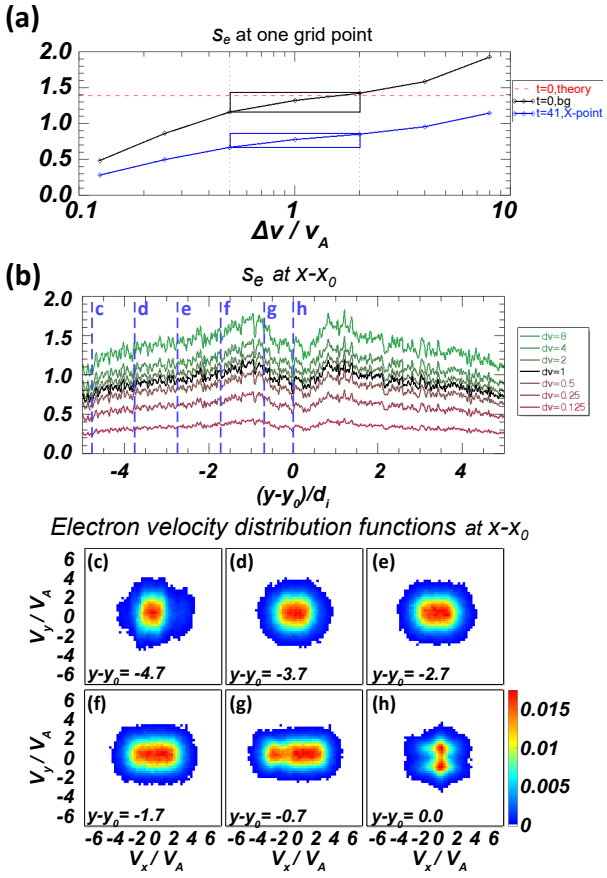

Figure 3. Velocity space grid dependence of local distribution functions. (a) Electron entropy density s_e as a function of velocity space grid Δv normalized to the Alfvén speed v_A. The black curve is s_e evaluated in the upstream region at $t = 0$. The blue curve is s_e at the X-point at $t = 41\ \Omega_{ci}^{-1}$. The red dashed line is the theoretical s_e upstream at $t = 0$. (b) Electron entropy density s_e as a function of the normal direction y in a cut across the X-point. Different colors indicate different velocity space grid Δv. The black curve is calculated with the selected velocity space grid $\Delta v = v_A \simeq 0.69 v_{th,e}$. (c)-(h) Reduced electron velocity distribution functions in the $v_x - v_y$ plane at $x - x_0 = 0$ and $y - y_0 = -4.7, -3.7, -2.7, -1.7, -0.7, 0.0 d_i = v_A/\Omega_{ci}$, denoted by the blue vertical dashed lines in panel (b), where the X-point location is (x_0, y_0).

of the fact that the late time distribution function has structures in velocity space that are not likely being completely resolved. For comparison, the change in the kinetic entropy between $t = 0$ and $t = 41\ \Omega_{ci}^{-1}$ is approximately a factor of 2, from about 1.3 far upstream of the current sheet at $t = 0$ to about 0.7 for the meandering electrons at the X-point at $t = 41\ \Omega_{ci}^{-1}$. The 15% uncertainty introduced by the velocity space grid resolution is considerably smaller than the physical change in kinetic entropy value of nearly a factor of 2, so this level of uncertainty is likely to often be sufficient to resolve physical changes in kinetic entropy.

We repeat this procedure for other distributions. Namely, we calculate the electron kinetic entropy density s_e along a slice in the inflow (y) direction through the X-point located at y_0 at $t = 41\ \Omega_{ci}^{-1}$, and plot the result as a function of velocity space grid Δv in Fig. 3(b). Six corresponding electron distribution functions at the locations marked by blue dashed lines in panel (b) are plotted in Figs. 3(c)-(h). Far upstream in panels (c) and (d), the distribution functions are close to Maxwellian, as expected. Closer to the X-point in panels (e), (f) and (g), the distribution functions are elongated along the local magnetic field direction, consistent with the trapped electron distributions discussed by Egedal and colleagues (*e.g.,* [65]). At the X-point in panel (h), as mentioned previously, the distribution function shows signatures of meandering motion. Even though these six distribution functions are very different, the selected velocity space grid $\Delta v = 1\ v_A \simeq 0.69\ v_{th,e}$ is in a medium range where the kinetic entropy is not strongly dependent on the velocity space grid, as shown in panel (b). The uncertainty at other locations is smaller than that at the X-point, as expected. This local analysis suggests that the velocity space grid resolution introduces $\simeq 15\%$ error in entropy calculated at later times when distribution functions can be strongly non-Maxwellian, but this error is smaller than the physical changes to the kinetic entropy, at least for the simulation study presented here.

4. Conclusions

In this study, we have investigated numerical aspects of the calculation of kinetic entropy in a collisionless particle-in-cell simulation. In Study 1 [46], it was shown that numerical effects led to the monotonic increase in measured kinetic entropy, which reproduces this important property of a physical collision operator. Here, assuming a relaxation time collision operator of Bhatnagar-Gross-Krook type that is local in space and time, we derive a relation between the numerical kinetic entropy time rate of change and the effective collision frequency. Calculating the kinetic entropy in the simulation then allows one to calculate the effective collision frequency in the collisionless PIC simulation. For the simulation in Study 1, the effective collision frequency is $\simeq 0.1\ \Omega_{ci}$.

This is an important step for future investigations of physical dissipation in PIC simulations. In particular, this approach allows one to estimate the effective collision frequency, so that one knows approximately how strong a physical collision operator has to be in order to overcome numerical effects. Modeling real collisions in PIC simulations requires the implementation of a physical collision operator into one's PIC code, as has been carried out previously (*e.g.,* [66, 67]).

This result raises important questions about the fidelity of collisionless PIC simulations. The simulation in Study 1, which was optimized with smaller than usual time step and spatial grid scale and a reasonably high number of macro-particles per grid, had an effective collision frequency of $0.1\ \Omega_{ci}$. This suggests that even a well-optimized collisionless PIC simulation carried out for hundreds of ion cyclotron times could have numerical dissipation play a significant role in the dynamical evolution of the system as particles effectively undergo numerous effective collisions. The situation would be even worse for simulations with fewer macro-particles per grid. On the other hand, macro-particles likely spend only a small amount of time in regions for which numerical collisionality is expected to be important, so it is possible that the dynamical effect of effective collisions is small. The excellent agreement between simulated distribution functions and *in situ* satellite observations of magnetic reconnection (*e.g.,* [68]) also suggests that the effect of numerical collisions is not likely very significant, but it is not clear this would be the case for a long duration simulation of a turbulent system or for collisionless shocks. Future work on this topic would be beneficial.

We also stress that the effective collision operator should not be overly interpreted as a physical collision process. We have not attempted to check if the evolution of distribution functions evolve according to the chosen collision operator, and in fact we expect a hypothetical collision operator mimicking the numerical effects would be much more complicated than the relaxation time approximation. Rather, the approach here is intended to merely be an effective model of the kinetic entropy increase due to numerical effects, especially in collisionless PIC simulations, and should be interpreted with the same caution as estimates of the effective numerical resistivity in magnetohydrodynamics (MHD) simulations.

While we stress that interpreting the numerical effective collision frequency too strictly is not appropriate, we believe it is instructive to estimate what the effective collision frequency we obtain corresponds to in physical systems of interest. For a typical solar active region magnetic field of 100 G the effective collision frequency from this simulation is $\simeq 10^6\ \Omega_{ci}$, while for a typical dayside magnetopause magnetic field of 40 nT it is $4\ \Omega_{ci}$. The actual (Spitzer) collision frequencies in these settings are $\simeq 6\times10^{-8}\ \Omega_{ci}$ and $10^{-15}\ \Omega_{ci}$, respectively. The effective collision frequency in the PIC simulations is, of course, far larger than the realistic values as expected, exemplifying how extremely rare collisions are in these systems. However, the estimated PIC effective collision frequency is orders of magnitude smaller than that in global magnetospheric MHD simulations, *e.g.,* $\simeq 3\times10^{11}\ \Omega_{ci}$ in Ref. [54], as expected.

A second activity of the present study is to assess the uncertainty of the kinetic entropy calculation in PIC simulations. Study 1 had shown that a velocity space grid close to the species thermal speed was sufficient to be close to the analytical predictions for a plasma with

exclusively Maxwellian distributions, but did not address the accuracy of the kinetic calculations as distributions evolve in time away from Maxwellians. Here, we confirm that kinetic entropy measurements are extremely sensitive to the velocity space grid if it is too large or too small, but there is a range around the thermal speed where the kinetic entropy is not so sensitive to the velocity space grid. Moreover, the changes in kinetic entropy measured in this range vary by approximately 15%, while the physical changes in kinetic entropy of a plasma going from the upstream region to the current sheet region were comparable to a factor of 2. We conclude a velocity space grid comparable to the thermal speed is sufficient to resolve physical changes to the kinetic entropy, at least for the simulation in Study 1.

There are many avenues for future work on these matters. For the estimate of the effective collision frequency, dependence on numerical quantities including time step, spatial grid scale, velocity space grid, macro-particles per grid, and speed of light would be useful. It would be interesting to use a PIC code with a physical collision operator to compare the effective collision frequency derived by the method used here with the physical value. Studies of more complicated systems than the basic magnetic reconnection simulation considered here, including plasma turbulence and shocks, would also be interesting. The dependence on velocity space grid should also be investigated as a function of the same numerical parameters and in different settings.

Acknowledgments

We acknowledge helpful conversations with S. P. Gary, M. A. Shay, and G. P. Zank. HL acknowledges support from NSF EPSCoR RII-Track-1 Cooperative Agreement OIA-1655280 and an NSF/DOE Partnership in Basic Plasma Science and Engineering via NSF grant PHY-1707247. PAC gratefully acknowledges support from NSF Grant PHY-1804428 and NASA Grant NNX16AG76G. MS acknowledges support from NASA grant 80NSSC19K0396. SS acknowledges funding from the European Unions Horizon2020 research and innovation programme under grant agreement No. 776262 (AIDA, www.aida-space.eu). This research uses resources of the National Energy Research Scientific Computing Center (NERSC), a DOE Office of Science User Facility supported by the Office of Science of the U.S. Department of Energy under Contract No. DE-AC02-05CH11231.

References

[1] Drake J F, Swisdak M, Schoeffler K M, Rogers B N and Kobayashi S 2006 *Geophys. Res. Lett.* **33** L13105
[2] Hesse M, Neukirch T, Schindler K, Kuznetsova M and Zenitani S 2011 *Space Sci. Rev.* **160** 3
[3] Cassak P A 2016 *Space Weather* **14** 186
[4] Cranmer S R 2002 *Space Sci. Rev.* **101** 229
[5] Parashar T N, Shay M A, Cassak P A and Matthaeus W H 2009 *Phys. Plasmas* **16** 032310
[6] Krall N A 1997 *Adv. Space Res.* **20** 715
[7] Howes G G 2018 *Phys. Plasmas* **25** 055501
[8] Boltzmann L 1877 *Wiener Berichte* **76** 373–435 in (Boltzmann 1909) Vol. II, paper 42.
[9] Bellan P M 2008 *Fundamentals of Plasma Physics* (Cambridge University Press)
[10] Erickson G M and Wolf R A 1980 *Geophys. Res. Lett.* **7** 897
[11] Borovsky J E, Thomsen M F, Elphic R C, Cayton T E and McComas D J 1998 *J. Geophys. Res.* **103** 20,297
[12] Kaufmann R L and Paterson W R 2006 *J. Geophys. Res.* **111** A10214
[13] Wolf R A, Kumar V, Toffoletto F R, Erickson G M, Savoie A M, Chen C X and Lemon C L 2006 *J. Geophys. Res.* **111** A12218
[14] Birn J, Hesse M, Schindler K and Zaharia S 2009 *J. Geophys. Res.* **114** A00D03
[15] Wolf R A, Wan Y, Xing X, Zhang J C and Sazykin S 2009 *J. Geophys. Res.* **114** A00D05
[16] Johnson J R and Wing S 2009 *J. Geophys. Res.* **114** A00D08
[17] Wang C P, Lyons L R, Wolf R A, Nagai T, Weygand J M and Lui A T Y 2009 *J. Geophys. Res.* **114** A00D02
[18] Sanchez E R, Wing S, Spanswick E and Donovan E 2012 *J. Geophys. Res.* **117** A05226
[19] Liu Y H, Birn J, Daughton W, Hesse M and Schindler K 2014 *J. Geophys. Res.* **119** 9773
[20] Du S, Zank G P, Li X and Guo F 2020 *Phys. Rev. E* **101** 033208

[21] Krommes J A and Hu G 1994 *Phys. Plasmas* **1** 3211–3238
[22] Howes G G, Cowley S C, Dorland W, Hammett G W, Quataert E and Schekochihin A A 2006 *Ap. J.* **651** 590
[23] Schekochihin A, Cowley S, Dorland W, Hammett G, Howes G, Quataert E and Tatsuno T 2009 *Ap. J. Supp. Ser.* **182** 310
[24] Loureiro N F, Schekochihin A A and Zocco A 2013 *Phys. Rev. Lett.* **111** 025002
[25] Numata R and Loureiro N F 2015 *J. Plasma Phys.* **81** 305810201
[26] Watanabe T H and Sugama H 2004 *Phys. Plasmas* **11** 1476
[27] Tatsuno T, Dorland W, Schekochihin A, Plunk G, Barnes M, Cowley S and Howes G 2009 *Phys. Rev. Lett.* **103** 015003
[28] TenBarge J M and Howes G G 2012 *Phys. Plasmas* **19** 055901
[29] Nakata M, Watanabe T H and Sugama H 2012 *Phys. Plasmas* **19** 022303
[30] TenBarge J M and Howes G G 2013 *Ap. J. Lett.* **771** L27
[31] Told D, Jenko F, TenBarge J, Howes G and Hammett G 2015 *Phys. Rev. Lett.* **115** 025003
[32] Li T C, Howes G G, Klein K G and TenBarge J M 2016 *Ap. J. Lett.* **832** L24
[33] Klein K G, Howes G G and TenBarge J M 2017 *J. Plasma Phys.* **83** 535830401
[34] Grošelj D, Cerri S S, Navarro A B, Willmott C, Told D, Loureiro N F, Califano F and Jenko F 2017 *Ap. J.* **847** 28
[35] Scudder J and Daughton W 2008 *J. Geophys. Res. Space Phys.* **113**
[36] Aunai N, Hesse M, Zenitani S, Kuznetsova M, Black C, Evans R and Smets R 2013 *Phys. Plasmas* **20** 022902
[37] Swisdak M 2016 *Geophys. Res. Lett.* **43** 43
[38] Kaufmann R L and Paterson W R 2009 *J. Geophys. Res.* **114** A00D04
[39] Kaufmann R L and Paterson W R 2011 *J. Geophys. Res.* **116** A08206
[40] Balasis G, Daglis I A, Papadimitriou C, Kalimeri M, Anastasiadis A and Eftaxias K 2009 *J. Geophys. Res.* **114** A00D06
[41] Leubner M P 2004 *Phys. Plasmas* **11** 1308
[42] Olivier C P, Engelbrecht N E and Strauss R D 2019 *J. Geophys. Res. Space Phys.* **124** 4–18
[43] Hammett G W and Perkins F W 1990 *Phys. Rev. Lett.* **64** 3019
[44] Eyink G L 2018 *Phys. Rev. X* **8** 041020
[45] Gary S P, Zhao Y, Hughes R S, Wang J and Parashar T N 2018 *Ap. J.* **859** 110
[46] Liang H, Cassak P A, Servidio S, Shay M A, Drake J F, Swisdak M, Argall M R, Dorelli J C, Scime E E, Matthaeus W H, Roytershteyn V and Delzanno G L 2019 *Phys. Plasmas* **26** 082903
[47] Antiochos S K, DeVore C R and Klimchuk J A 1999 *Ap. J.* **510** 485
[48] Tóth G, van der Holst B, Sokolov I V, Zeeuw D L D, Fang T I G F, Manchester W B, Meng X, Najib D, Powell K G, Stout Q F, Glocer A, Ma Y J and Opher M 2012 *J. Comput. Phys.* **231** 870
[49] Siscoe G L, Erickson G M, Sonnerup B U Ö, Maynard N C, Schoendorf J A, Siebert K D, Weimer D R, White W W and Wilson G R 2002 *Geophys. Res. Lett.* **29** 1626
[50] Lyon J G, Fedder J A and Mobarry C M 2004 *J. Atmos. Sol. Terr. Phys.* **66** 1333
[51] Raeder J, Larson D, Li W, Kepko E L and Fuller-Rowell T 2008 *Space Sci. Rev.* **141** 535
[52] Janhunen P, Palmroth M, Laitinen T, Honkonen I, Juusola L, Facskó G and Pulkkinen T I 2012 *J. Atmos. Sol. Terr. Phys.* **80** 48
[53] Press W H, Teukolsky S A, Vetterling W T and Flannery B P *Numerical Recipes in Fortran 77*
[54] Komar C M, Cassak P A, Dorelli J C, Glocer A and Kuznetsova M M 2013 *J. Geophys. Res.* **118** 4998–5007
[55] Dawson J 1962 *Phys. Fluids* **5** 445
[56] Dawson J 1964 *Phys. Fluids* **7** 419
[57] Montgomery D and Nielson C W 1970 *Phys. Fluids* **13** 1405
[58] Hockney R W 1971 *J. Comput. Phys.* **8** 19
[59] Turner M M 2006 *Phys. Plasmas* **13** 033506
[60] Lai P Y, Chen L, Lin-Liu Y R and Chen S H 2015 *Phys. Plasmas* **22** 092127
[61] Bhatnagar P L, Gross E P and Krook M 1954 *Phys. Rev.* **94** 511
[62] Greco A, Valentini F, Servidio S and Matthaeus W H 2012 *Phys. Rev. E* **86** 066405
[63] Servidio S, Chasapis A, Matthaeus W, Perrone D, Valentini F, Parashar T, Veltri P, Gershman D, Russell C, Giles B *et al.* 2017 *Phys. Rev. Lett.* **119** 205101
[64] Ng J, Egedal J, Le A, Daughton W and Chen L J 2011 *Phys. Rev. Lett.* **106** 065002
[65] Egedal J, Le A and Daughton W 2013 *Phys. Plasmas* **20** 061201
[66] Daughton W, Roytershteyn V, Albright B J, Karimabadi H, Yin L and Bowers K J 2009 *Phys. Rev. Lett.* **103**(6)
[67] Daughton W, Roytershteyn V, Albright B J, Karimabadi H, Yin L and Bowers K J 2009 *Phys. Plasmas* **16** 072117

[68] Burch J L, Torbert R B, Phan T D, Chen L J, Moore T E, Ergun R E, Eastwood J P, Gershman D J, Cassak P A, Argall M R, Wang S, Hesse M, Pollock C J, Giles B L, Nakamura R, Mauk B H, Fuselier S A, Russell C T, Strangeway R J, Drake J F, Shay M A, Khotyaintsev Y V, Lindqvist P A, Marklund G, Wilder F D, Young D T, Torkar K, Goldstein J, Dorelli J C, Avanov L A, Oka M, Baker D N, Jaynes A N, Goodrich K A, Cohen I J, Turner D L, Fennell J F, Blake J B, Clemmons J, Goldman M, Newman D, Petrinec S M, Trattner K J, Lavraud B, Reiff P H, Baumjohann W, Magnes W, Steller M, Lewis W, Saito Y, Coffey V and Chandler M 2016 *Science* **352** 6290